IAA-AAS-DyCoSS 4-5-17
AAS 18-621

AN ANALYSIS OF THE PORKCHOP PLOT FOR DIRECT, MULTI-REVOLUTION AND FLYBY MISSIONS

Davide Menzio[*] and Camilla Colombo[†]

Abstract. The porkchop plot is an extremely useful tool that was developed to efficiently identify families of trajectories with low characteristic energy difference, over different launch/arrival dates and time of flights for a specific interplanetary journey. This preliminary trajectory modeling has been applied to several and successful missions, Voyager included, however, in authors opinion, it has never been fully exploited nor deeply investigated. Indeed, general applications focus the attention only to minimum solutions while high delta-vs are not questioned.

In this paper, a thorough analysis for direct and multi-revolutions trajectories is performed and investigates the location and the shape of the minimum. Purely geometric relations enable a quick identification of the minimum solution. It is possible therefore to constrain the resolutions of the Lambert's problem to a confidence region around the minimum, avoiding to run unnecessary simulations.

An analysis of gravity assists for direct transfer, extensible to the multi-revolution one, is performed by stacking porkchops one on an another in the 3D space. This can be done in a purely graphical way, considering the specific energy at departure and arrival and the surfaces associated to how well the infinity velocities patch at the flyby.

In the end, a tool to further constrain the search space for the post-encounter leg is obtained by studying the maximum/minimum variations of the semi-major axis and eccentricity induced by close/distant encounter with the respect to their desired value.

The purpose of this paper is to show that, when direct solutions produce unfeasible results, multi-revolutions are always possible. Secondarily, a quick way to represent gravity assist trajectories on the 3D porkchop plot is presented and compared with the solution offered by the search space identification tool.

INTRODUCTION

Despite porkchop plots are generally associated to the Mars exploration era, their first use dates back to the Voyager missions,[1] when analysts developed the chart with the specific purpose of intercepting Saturn within 1981 but avoiding close encounters either on Thanksgiving or Christmas. In their most common application, porkchop plots represent the characteristic energy (C_3) associated to different departure and arrival conditions for a specific targeting problem and it is its distinctive shape, resembling indeed a steak, which earned the chart such a peculiar name.[1]

[*]PhD student, Department of Aerospace Science and Technology, Politecnico di Milano, via la Masa, 34, 20154, Milano (IT).

[†]Associate professor, Department of Aerospace Science and Technology, Politecnico di Milano, via la Masa, 34, 20154, Milano (IT).

Indeed, these plots show the solutions of the classical Lambert's problem: at each pair of departure and arrival dates are associated two positions and a time of flight whose solution is a conic, expressed in term of classical keplerian elements, as it can be seen in Eq.(1):

$$\begin{aligned} \sqrt{\tfrac{\mu}{a^3}}\Delta t &= \alpha - \beta - (\sin\alpha - \sin\beta) \\ \sin\alpha = \sqrt{\tfrac{s}{2a}} \quad \sin\beta &= \sqrt{\tfrac{s-c}{2a}} \end{aligned} \tag{1}$$

where the semi-major axis, a, is solved numerically from the non-linear equation (1), function of the time of flight, Δt, the standard gravitational parameter, μ, and two terms the semi-perimeter s and the chord c of the so called space triangle which depend only on the departure and arrival positions.[2] It is clear how each point in a porkchop plot corresponds to a solution of the Lambert problem, and therefore how an enormous number of computations is required to discover all the possible trajectories available for a predefined mission scenario.

Porkchop plots are an extremely useful visualization tool that allow mission planners to analyse and evaluate the transfer orbits with the respect of different performance parameters such as: characteristic energy at the departure and at the arrival, total delta-v, transfer duration, maximum distance to Sun, etc.[3] An extensive literature about this subject doesn't exist alone and it is generally associated to studies on the Lambert's problem and it's extension,[4,5] or to specific mission.[6,7]

Despite more than four decades of use, we believe that the porkchop plot is generally not employed at its full potential and also it could be created from a restricted search space, avoiding unnecessary computations for solutions that are known a priori to be not optimal. It could include additional minima if multi-revolution transfer are considered and it could provide a comprehensive map to assess the time schedule for a possible flyby mission or used to constrain the time grid of a leg, considering the arrival condition of the previous and the effect of the flyby. The problem represented by the gravity assisted trajectory, in particular, is complex to be evaluated from the single porkchop plots associated to in-/outbound legs and require the linear combination of the two solutions at given date of flyby. Which explain the interest in handle such a problem in a more graphically related way.

The paper is organized as follows: in section 2, a thorough analysis of the porkchop is provided in order to investigate the location and the shape of minimum solutions. In section 3, the direct transfer is extended to the multi-revolution case and the latter solutions are stacked one top of the other showing how the single revolution porkchop plot can be filled with new minima. To conclude, a 3D porkchop for the single flyby problem is generated in section 4 and it is shown how it can be used to reduce the the search space in correspondence of two interplanetary legs including a single flyby in section 5.

ANALYSIS OF THE CLASSICAL PORKCHOP PLOT

In order to have a clear understanding on the solution displayed by the porkchop, some simplification must be introduced. Therefore, departure and arrival planets are here considered to lay on circular and coplanar trajectories ensuring smoother contours of the delta-v, see Fig.1.

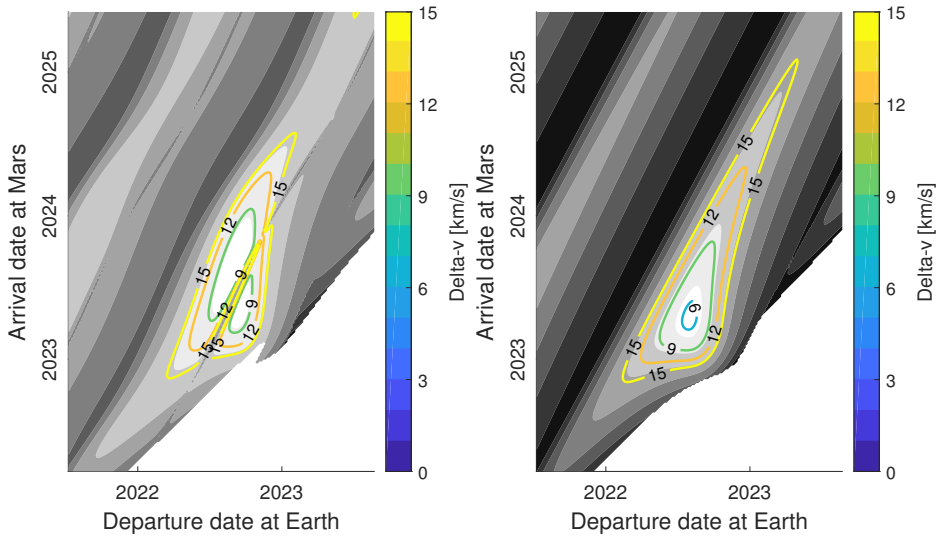

Figure 1: The porkchop plot for a Earth-Mars transfer opportunity, obtained considering real (left) and simplified (right) dynamics. Considering the orbit circular and coplanar allows to an easier analysis of the the location and shape of the minima, avoiding to deal with secondary effects which soil the smooth contours, i.e. the inclination induces the presence of the central ridge[3,6]

In such configuration, it is possible to observe that the center of the valley is the solution for the Hohmann transfer, identified in Fig.2 at the intersection of the red dashed lines. Such representation allows to show that the solution repeats with a specific frequency, associated to the synodic period, defined in Eq.2:

$$P_{syn} = \frac{2\pi}{\sqrt{\frac{\mu}{a_{dep}^3}} - \sqrt{\frac{\mu}{a_{arr}^3}}} \tag{2}$$

computed as the difference of mean motions related to departure and arrival planets.
As expected, the location of the minimum solutions is predictable and located at the intersection between two lines:

- the π-line;
- the t_H-line.

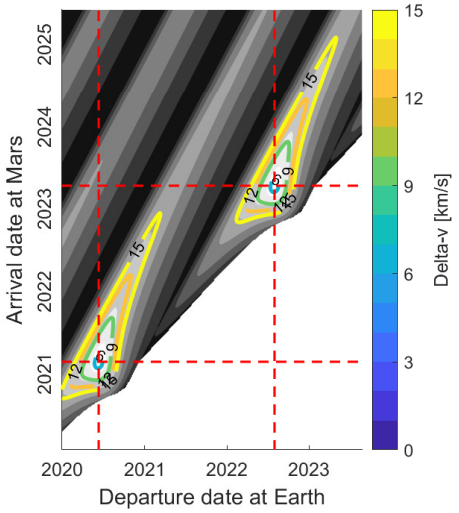

Figure 2: The center of the minimum delta-v contour, identified by the red dashed lines, repeats every synodical period

With the former, we identify the locus of points in which the phasing angle individuated by the position vectors of the departure and arrival planets is exactly π, see Fig.3, while the latter where the time of flight is half period of the Hohmann transfer, see Fig.4, defined by Eq.3:

$$P_H = \frac{\pi}{\sqrt{\frac{2\mu}{(a_{dep}+a_{arr})^3}}} \tag{3}$$

The intersection between the π-lines and t_H-lines determines exactly when Hohmann transfer can take place in terms of departure and arrival dates and explain also the repetitiveness of the solution with the synodical period, see Fig.5.

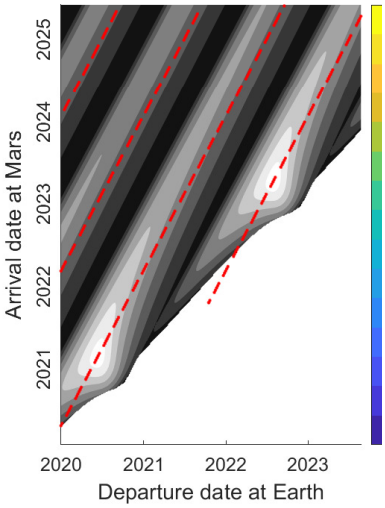

Figure 3: The π-lines

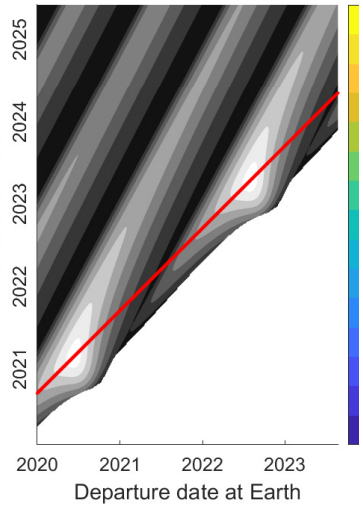

Figure 4: The t_H-line

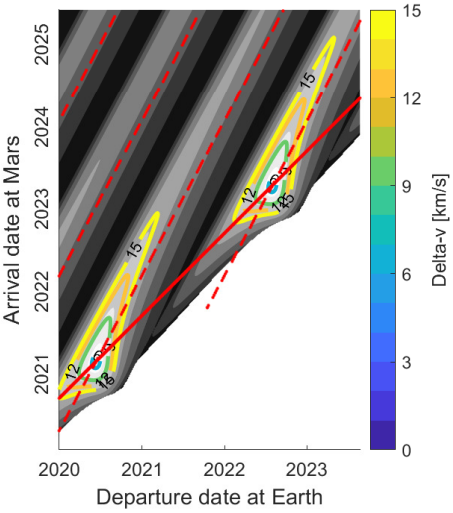

Figure 5: The identification of the center of the minimum at the intersection of π- and t_H-lines

Now that the delta-v can be restricted to a neighborhood of the minimum valley, it is interesting to study how the contours assume their characteristic triangular shape. Fig.8 displays how the characteristic energy at the departure, see Fig.6, and at the arrival, see Fig.7, sums up to generate the delta-v triangle. The difference between the shape of the infinite velocity level is explained by representing the transfer orbit associated to the contour and studying the departure/arrival velocity configuration with the respect of the initial/final orbit.
It is clear how the total delta-v is the smoothed solution of the two.

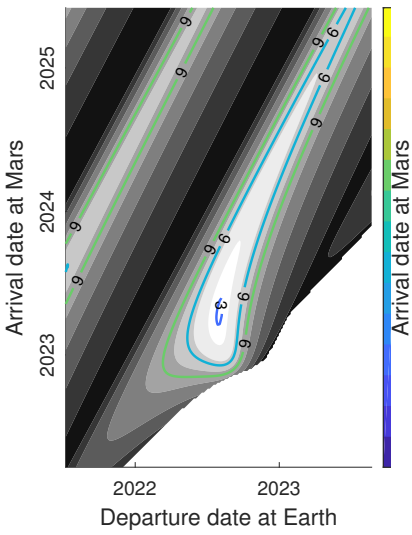

Figure 6: The characteristic energy at the departure, C_3^{dep}

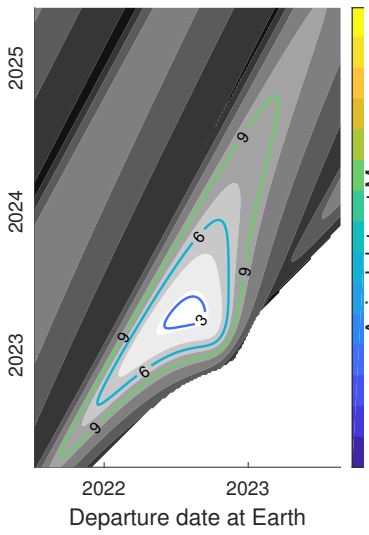

Figure 7: The characteristic energy at the arrival, C_3^{arr}

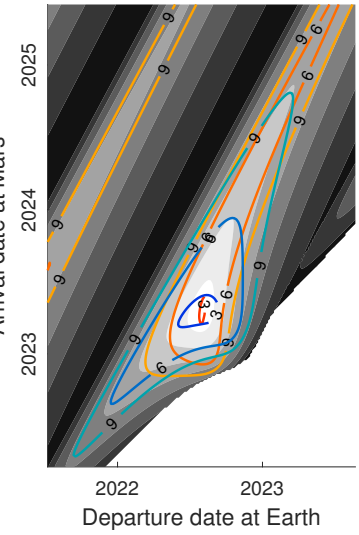

Figure 8: The delta-v contour as the sum of the specific energies

Although the characteristic energy could give a direct indication of the difference in magnitude and direction of the manoeuvres that must be performed, the representation of the semi-major axis and of the eccentricity in the porkchop plot allows for an immediate interpretation of the reason why minimum solutions occurs in a triangular shape.

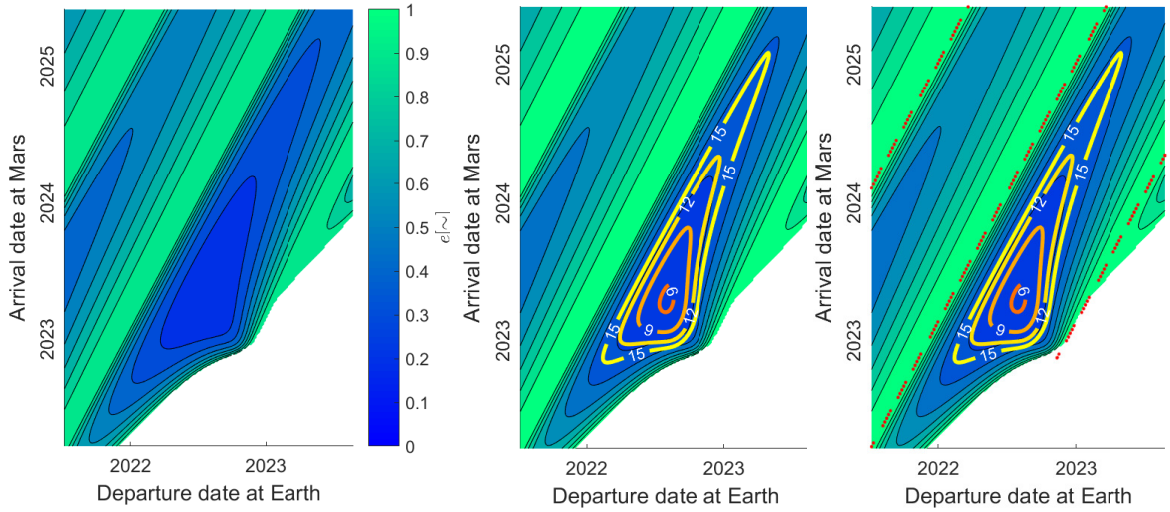

Figure 9: The trend of the eccentricity isolines over the contour of the delta-v minima and the locus of the point at phasing 0 (red dashed lines)

As it can be seen from Fig.9, the contour of the minima resembles quite accurately the chart of the eccentricity, however it looks a bit more elongated in the direction of the π-line and compressed by the 0-lines.

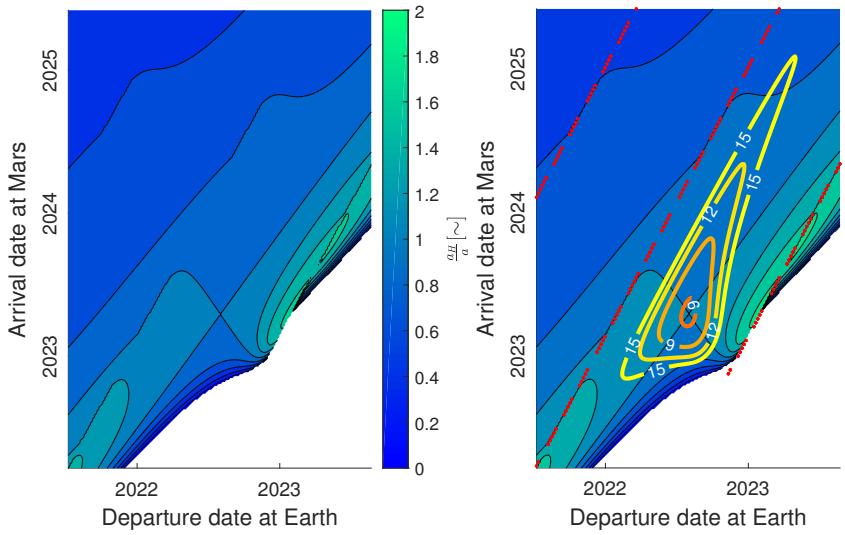

Figure 10: The trend of the the semi-major axis isolines, represented through its inverse scaled on the value obtained for the Hohmann transfer, over the contour of the delta-v minima and the locus of the point at phasing 0, represented with the red dot lines

Such behavior can be explained by giving a quick look to the semi-major axis contours, see Fig.10, which shows high values where the small phasing angle, 0-line, meet short time of flights, and thus the orbit approaches the parabolic trajectory. Therefore, despite the high eccentricity of

the transfer trajectory, obtained for the upper lobe of the triangle, a reasonable low semi-major axis ensures a low delta-v.

FROM THE DIRECT TO THE MULTI-REVOLUTION PORKCHOP PLOT

Introducing a modification of the t_H-lines (from the locus of the points where the time of flight is half of the Hohmann period to an odd multiple of the Hohmann transfer time of flight) provides an intuitive reason for considering multi-revolution solutions falling thus in an increased search space.

Indeed, when the time of flight is high enough, in general, a multi-revolution trajectory is more efficient,[4,5] although it requires some forethought.

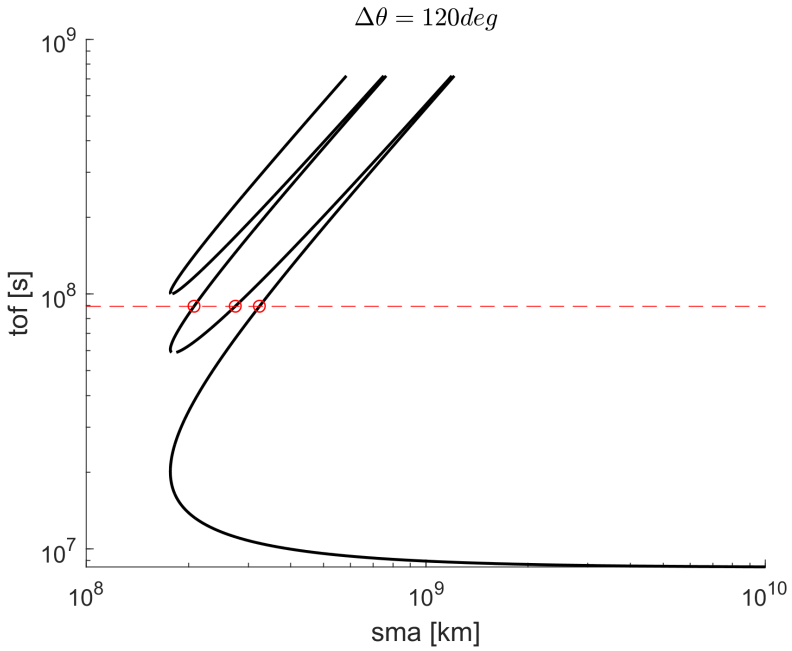

Figure 11: The multi-revolution plot displays the semi-major axis and the time of flight for the transfer arc connecting the departure and arrival planets in a specific configuration ($120\,\mathrm{deg}$).

Fig.11 shows that, for high enough time of flight, multi-revolution transfers are possible and present lower semi-major axis when compared with the direct solution. Moreover, there are two possible semi-major axis solutions that cannot be evaluated a-priori: in fact, when $\Delta\theta \leqslant \pi$, the upper branch corresponds to long transfer orbits, while the lower branch corresponds to the short one, and vice versa for $\Delta\theta > \pi$.[4]

The associated minimum solutions are still centered with the respect of the intersection between π-lines and kt_H-lines, where k is an odd number but presents a butterfly shape, with the lower-right lobe assigned to the long transfers associated to $\Delta\theta > \pi$ and with the upper-left one to the short ones associated to $\Delta\theta \leqslant \pi$, see Fig.12.

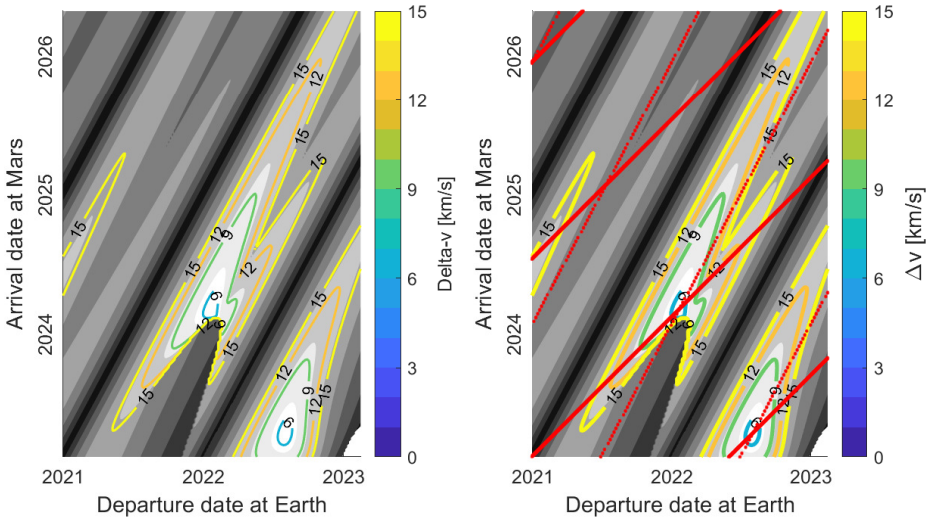

Figure 12: The delta-v contours associated to the direct and 1 revolution transfers: the butterfly shape obtained for the multi-rev trajectories is displayed above the triangular one of the direct (left), why both of the center of the delta-v valley are identified by the intersection of π- and kt_H-lines.

Similar evaluation of the shape can be made analysing the transfer eccentricity and semi-major axis, see Fig.13.

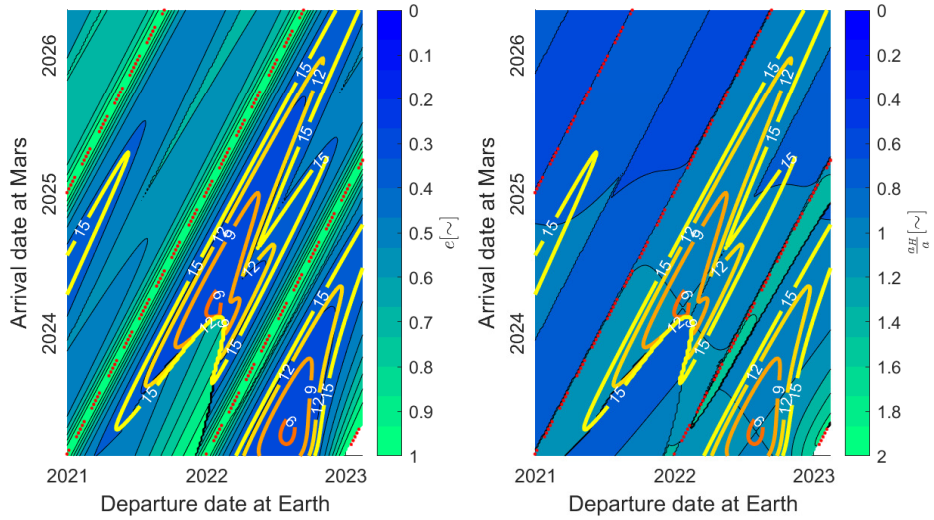

Figure 13: The shape of the delta-v valley explained from the trend of the eccentricity isolines (left) and the inverse semi-major axis scaled on the value obtained for the Hohmann transfer. The red dot line identifies the locus of the point where the phasing angle is 0

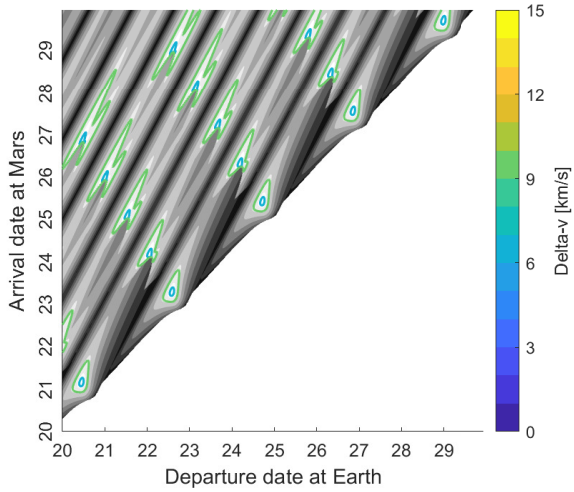

Figure 14: The direct and multi-revolution minimum delta-v contour, up to the 4th revolutions, represented in the porkchop plot

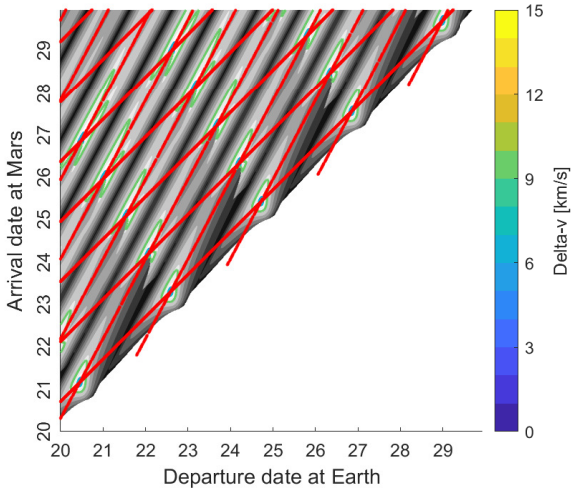

Figure 15: The identification of the center of minima, up to the 4th revolution, with the π- and kt_H-lines

Such considerations enables to open new scenarios to those identified by the direct transfer and to populate the porkchop of new minima, see Fig.14, whose center can be located with no need to resolve the associated Lambert's problem but exploiting the geometric criteria, see Fig.15.

THE 3D PORKCHOP PLOT FOR THE SINGLE FLYBY PROBLEM

Switching now from the direct transfer to a two-leg the flyby trajectory can be beneficial from the point of view of fuel/cost mission saving and the opportunity represented by new launch windows. Nevertheless, gravity assist requires a significant increase in the number of computations, in general quantifiable with a multiplicative factor n, for an $n-$ gravity assisted mission, assuming a similar time grid. From the point of view of trajectory analysis, this could also be problematic, since each porkchop cannot be evaluated anymore individually, but together with the others ensuring the "matching" between the boundary conditions at the flyby, expressed in term of in-/outbound infinity velocity.

The relative velocities at the flyby planet, $\mathbf{v}_\infty^\pm$, computed from the difference of the solutions of the two different Lambert's problem, $\mathbf{v}^\pm$, and the planet heliocentric velocity, $\mathbf{v_{pl}}$:

$$\begin{aligned} \mathbf{v}_\infty^- &= \mathbf{v}^- - \mathbf{v_{pl}} \\ \mathbf{v}_\infty^+ &= \mathbf{v}^+ - \mathbf{v_{pl}} \end{aligned} \tag{4}$$

identify two hyperbolic trajectories whose matching can be ensured by applying a manoeuvre at the sphere of influence. Infinite impulses are implemented so that to equal the difference of the in-/out-coming relative velocities:

$$\Delta v_\infty = \left| v_\infty^- - v_\infty^+ \right| \tag{5}$$

considering that an additional cost must be paid when the flyby does not provide the necessary contribution in term of desired turning angle:

$$\Delta v_\infty = \sqrt{{v_\infty^+}^2 + {v_\infty^-}^2 - 2v_\infty^+ v_\infty^- cos(\delta - \delta_{MAX})} \tag{6}$$

where δ is the angular distance between in-/outgoing infinite velocities and δ_{MAX} is defined from the minimum allowed periapsis passage $r_{p_{min}}$:[2,3,8]

$$\delta_{MAX} = \max_{v_\infty^+, v_\infty^-} \left(2\sin^{-1} \frac{1}{1 + \frac{r_{p_{min}} v_\infty^2}{\mu}} \right) \tag{7}$$

In order to evaluate the flyby we are required to study how the Lambert's solution for two legs recombine at the common planet, evaluating the difference of relative velocities and the turning angle required considering the maximum allowable, and the terminal points. The idea behind the 3D porkchop consists in the fact that such analysis could be performed directly in 3D, preserving the matrix structure of the data which enable its direct representation. In principle, it is possible to expand the characteristic energies at the departure and arrival planet in the third missing dimension of a graph and to combine these results with two indexes of merit for the flyby:

- the turning angle smaller than the maximum prescribed value, $\delta \leqslant \delta_{MAX}$;
- small infinity manouevre: ($\Delta v_\infty \leqslant 1 km/s$).

For the single flyby problem, it is possible to define the following reference for the 3D porkchop plot: assigning the x-, y- and z-axes respectively to the departure, flyby and arrival date. In such configuration, C_3^{dep} lays on the x-y plane and it has to be expanded in the z-axis, see Fig.16, while C_3^{arr} lays on the y-z plane and it has to be extended in the x-axis, as shown in Fig.17:

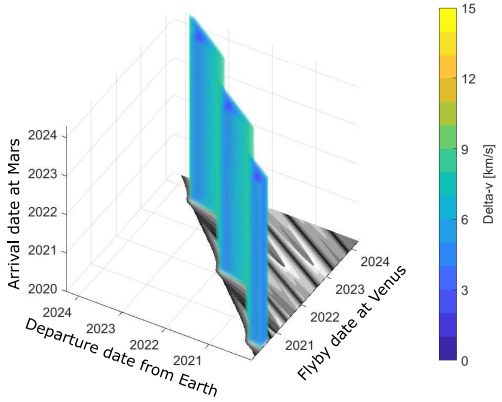

Figure 16: The expansion of C_3^{dep} along the z-axis

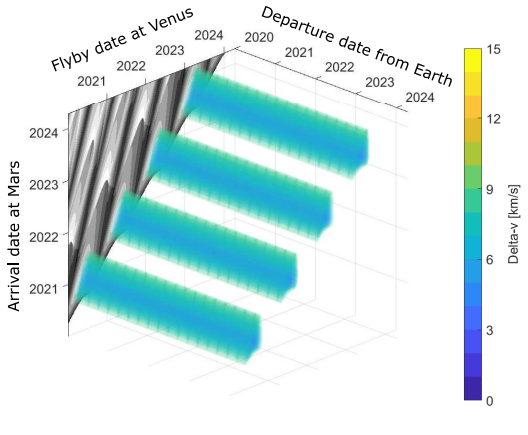

Figure 17: The expansion of C_3^{arr} along the x-axis

By themselves, the two 3D plot associated to the characteristic energy at the departure/arrival are meaningless, since they identify, in principle unfeasible transfer that doesn't respect the time law. Nevertheless, there is no need to worry since the combination of the two ensures the solution to be feasible, see Fig.18:

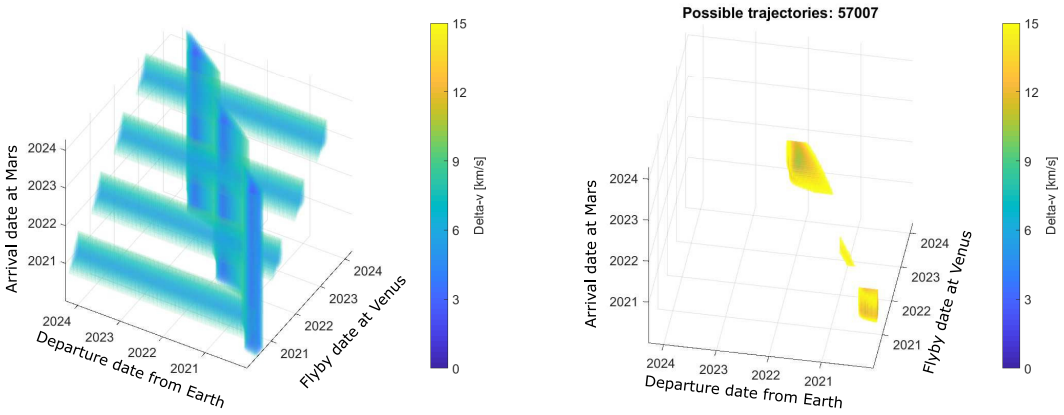

Figure 18: The intersection of C_3^{dep} and C_3^{arr}

The linear interpolation of the two is not enough to effectively constrain the solution in such three dimensional space, see Fig.18. Over 57000 possible trajectories are identified and additional constraints must be considered. The flyby must be considered and to do that two indexes of merit, which were previously identified, can be generated into 3D constraint surfaces which effectively reduce the feasible solution from about 60 thousand points to less than 4.5 thousand, see 20.

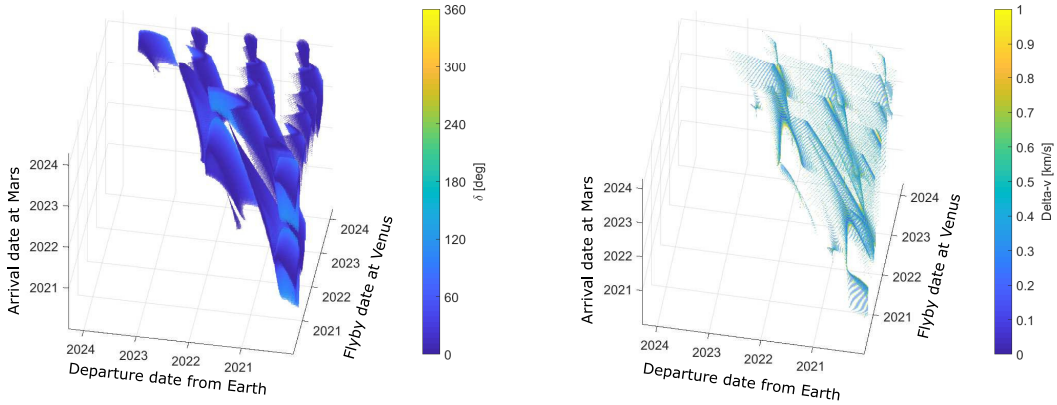

Figure 19: The 3D surfaces associated with the indexes of merit of the flyby: the admissible turning angle, δ, (left) and small difference between the relative velocities, Δv_∞, (right)

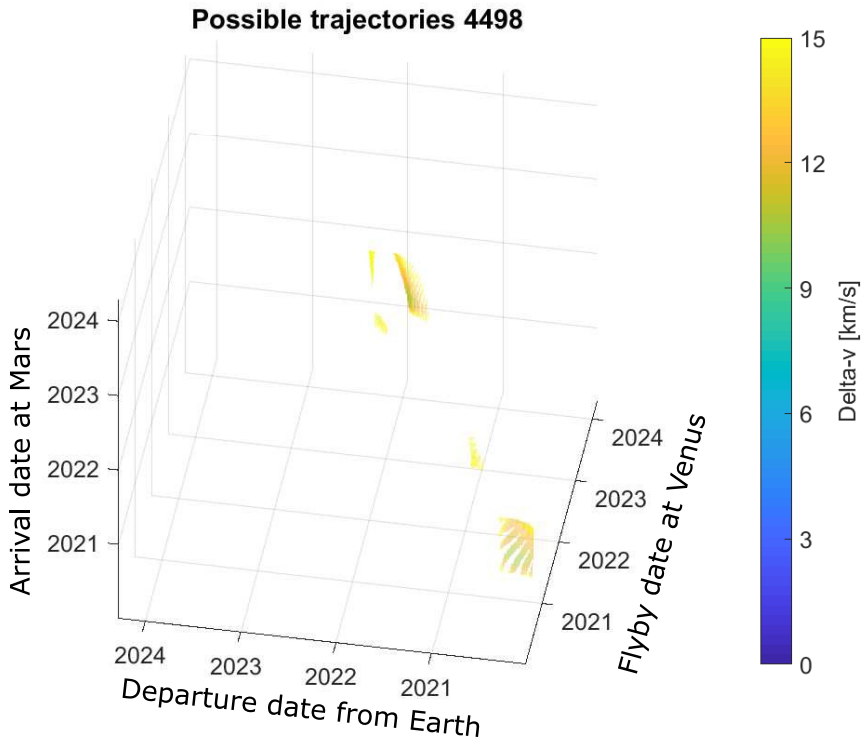

Figure 20: The final result of the 3D porkchop plot, obtained from the characteristic energy at departure and arrival, admissible turning angle, δ, and the small Δv_∞

AN APPLICATION OF THE 3D PORKCHOP PLOT TO CONSTRAINT THE SEARCH SPACE FOR FOLLOWING LEGS

Although the 3D porkchop plot could be an interesting graphical representation of flyby trajectories, it could be more useful for mission analysis purposes to combine the knowledge of the first leg, with the flyby effect, to constraint the search space for the following arc.

With the respect of the previous section, in which the two legs were computed separately and the flyby was studied as the result of the two, in this section the idea behind is to compute only the first leg and to consider the worst case for the flyby, from which it is possible to constrain the second leg two a specific area. In order to do that, starting from the relative velocity, obtained from the resolution of the Lambert's problem for the first leg, the flyby is studied in term of the deflection associated to the extreme cases of passage at the minimum allowed altitude of the periapsis or at the sphere of influence.

Defined the approach angle, f in Fig.21, between the relative velocity, $\mathbf{v}_\infty^-$, and the heliocentric one of the planet, $\mathbf{v_{pl}}$, as shown in Fig. 21:

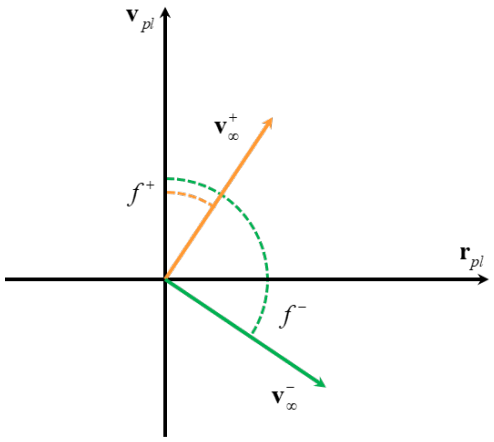

Figure 21: The approach angle defined between between the relative velocity, $\mathbf{v}_\infty^-$, and the heliocentric one of the planet, $\mathbf{v_{pl}}$

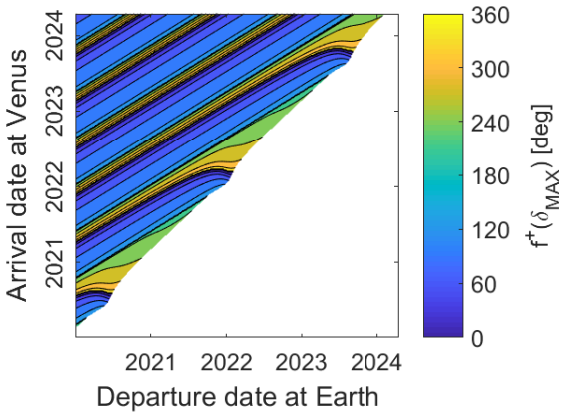

Figure 22: The entry angle for Venus encounter

Therefore, from the entry angle obtained from the resolution of the Lambert's problem for the first leg, here represented in Fig.22, and the upper and lower limit for the deflection angle, described by Eq.8:

$$\begin{aligned} \delta_{MAX} &= 2\sin^{-1}\left(1+\frac{r_{p_{min}}v_\infty^{-2}}{\mu}\right)^{-1} \\ \delta_{min} &= 2\sin^{-1}\left(1+\frac{r_{SOI}v_\infty^{-2}}{\mu}\right)^{-1} \end{aligned} \tag{8}$$

it is possible to estimate the outbound approach angle, $f^+ = f^- \mp \delta$ as you can see in Fig. 23, where $-$ or $+$ are derived considering only prograde motion for $f^- \leqslant \pi$ and $f^- > \pi$, respectively, see Fig.23.

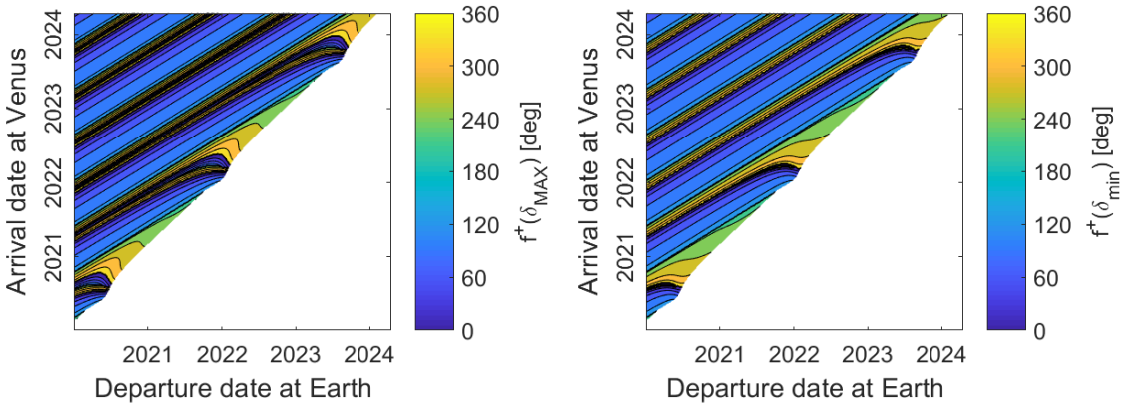

Figure 23: The exit angle, f^+, at Venus considering a passage at $r_{p_{min}}$, left, and r_{SOI}, right.

The associated outbound heliocentric velocities are determined from Eq.9 and here represented, see Fig.24:

$$\mathbf{v}_{\infty}^{+} = R_3\left(\mp\delta\right)\mathbf{v}_{\infty}^{-} \quad \mathbf{v}^{+} = \mathbf{v}_{\infty}^{+} + \mathbf{v}_{\mathbf{pl}} \tag{9}$$

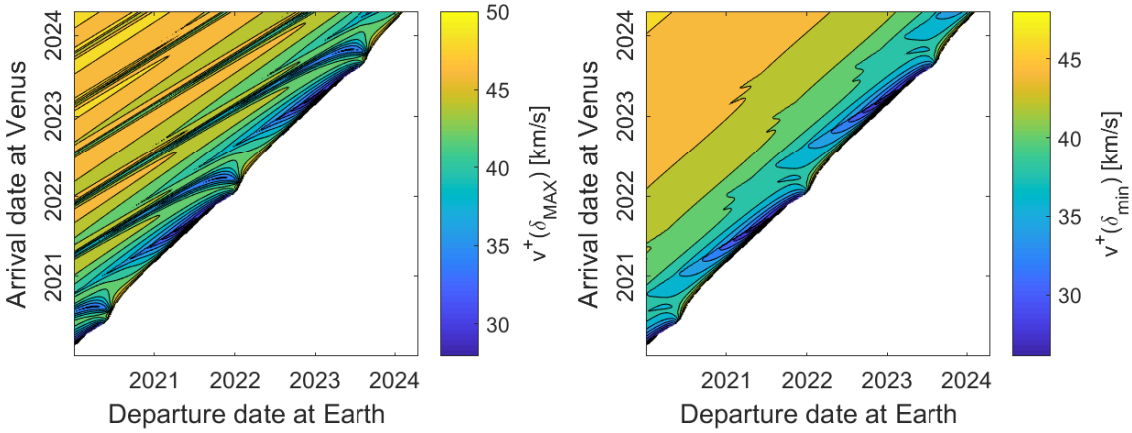

Figure 24: The heliocentric velocity, v^{+}, considering a passage at $r_{p_{min}}$, left, and r_{SOI}, right.

from which the keplerian elements of the heliocentric trajectory are determined, following Eq.10:

$$\begin{aligned} \mathbf{e} &= \frac{\left(v^{+2} - \frac{\mu}{r_M}\right)\mathbf{r_M} - \left(\mathbf{r_M}\cdot\mathbf{v}^{+}\right)\mathbf{v}^{+}}{\mu} \\ a &= \left(\frac{v^{+2}}{\mu} - \frac{2}{r_M}\right)^{-1} \quad e = \|\mathbf{e}\| \end{aligned} \tag{10}$$

the associated upper and lower limit estimated: for the semi-major axis, a, through Eq.11 and here represented, see Fig.25:

$$\begin{aligned} a_{ul} &= \max\left(a\left(\delta_{MAX}\right), a\left(\delta_{MIN}\right)\right) \\ a_{bl} &= \min\left(a\left(\delta_{MAX}\right), a\left(\delta_{MIN}\right)\right) l \end{aligned} \tag{11}$$

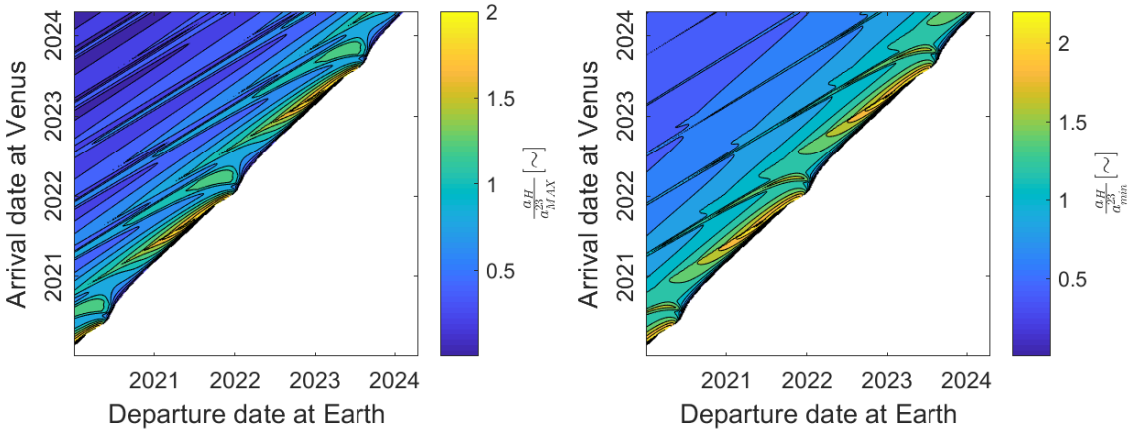

Figure 25: The upper (left) and lower (right) limit for the semi-major axis

and similarly for the eccentricity, e, see Fig.26.

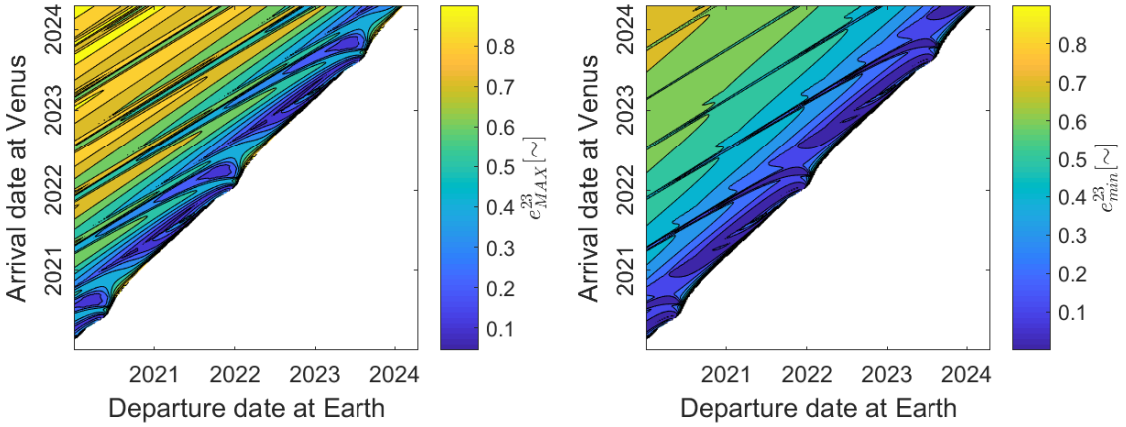

Figure 26: The upper (left) and lower (right) limit for the eccentricity

Comparing the expected/desired value of the transfer orbit with the limits in 3D, it is possible to show how the solution for the 3d porkchop plot is within the boundaries identified, see Fig.27.

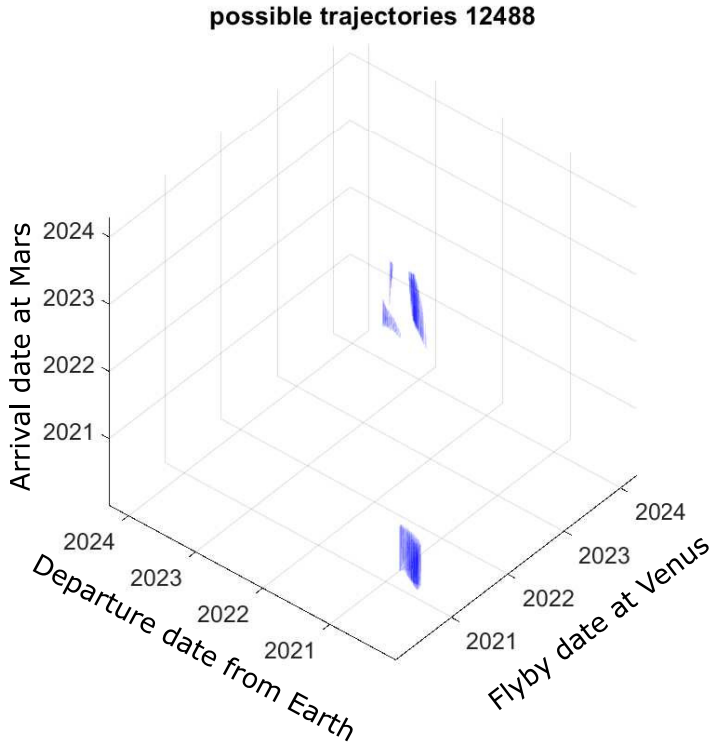

Figure 27: The representation of the feasible transfer obtained from the flyby analysis of the first leg

In the end, by shirking the system along the x-axis, it is possible to effectively constraint the search space from the full set of Lambert's problem solution to the restricted one, see Fig.28, avoiding unnecessary computations.

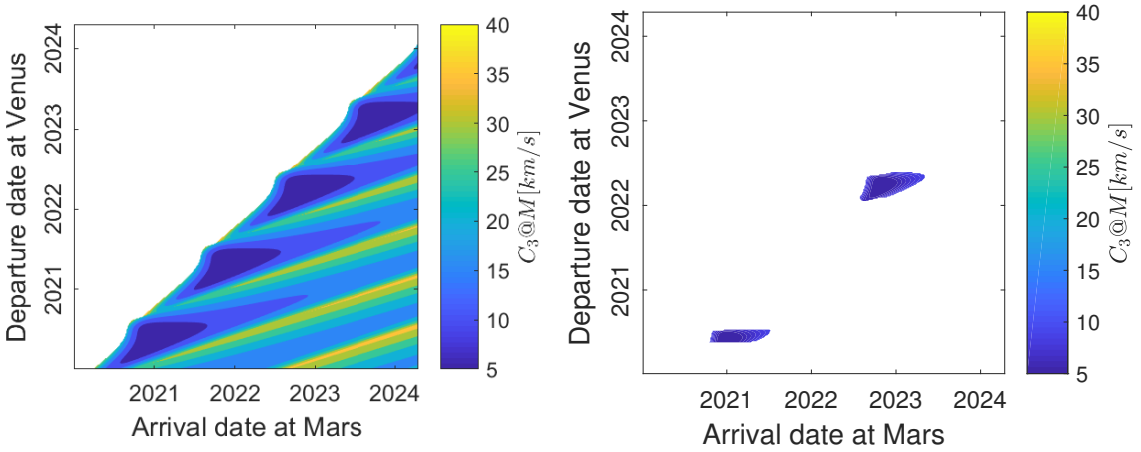

Figure 28

CONCLUSION

The porkchop was analysed for the classical direct transfer, refreshing how the minimum solutions can be localised considering purely geometric quantities and studying the shape of their contours. The porkchop plot was then extended to the multi-revolutions orbit, extending the localisation of the minima and the study of the shapes. A new graphical way to display flyby trajectories was offered through the 3d porkchop plot and used to "validate" the 3d masks obtained by studying the effects of the flyby applied to the pre-encounter porkchop plot to define the search space in the post-encounter one.

ACKNOWLEDGEMENT

The work performed with this paper has received funding from the European Research Council (ERC) under the European Union's Horizon 2020 research and innovation program (grant agreement No 679086 - COMPASS).

REFERENCES

[1] P. J. Westwick, *Into the black: JPL and the American space program, 1976-2004*. Yale University Press, 2008.
[2] J. E. Prussing and B. A. Conway, *Orbital mechanics*. Oxford University Press, USA, 1993.
[3] A. David, "Vallado. Fundamentals of Astrodynamics and Applications," 1997.
[4] H. Shen and P. Tsiotras, "Using Battin's method to obtain multiple-revolution Lambert's solutions," *Advances in the Astronautical Sciences*, Vol. 116, 2003, pp. 1067–1084.
[5] H. Shen and P. Tsiotras, "Optimal two-impulse Rendezvous between two circular orbits using Multiple-Revolution Lambert's Solutions," *AIAA Guidance, Navigation, and Control Conference and Exhibit*, 2002, p. 4844.
[6] R. C. Woolley and C. W. Whetsel, "On the nature of Earth-Mars porkchop plots," 2013.
[7] S. Matousek and A. Sergeyevsky, "To Mars and back-2002-2020: Ballistic trajectory data for the Mission Architect," *AIAA/AAS Astrodynamics Specialist Conference and Exhibit*, 1998, p. 4396.
[8] R. H. Battin, *An introduction to the mathematics and methods of astrodynamics*. Aiaa, 1999.